PERGAMON

International Journal of Multiphase Flow 25 (1999) 957–975

International Journal of Multiphase Flow

www.elsevier.com/locate/ijmulflow

The relation between the Taylor bubble motion and the velocity field ahead of it

S. Polonsky, L. Shemer, D. Barnea*

Department of Fluid Mechanics and Heat Transfer, Faculty of Engineering, Tel-Aviv University, Tel-Aviv 69978, Israel

Received 26 October 1998; received in revised form 26 March 1999

This paper is dedicated to Professor Gad Hetsroni on the occasion of his 65th birthday. Gad, through his leadership and devotion to science in general and multiphase flows in particular, has been the beacon of this field. As the Founder and the Editor of the *International Journal of Multiphase Flow*, Gad has marched this field forward at a rapid pace and positioned it at the focus of science and engineering. We would like to express our deep gratitude to Gad for all he has done for the field of multiphase flow and we wish him many more productive and enjoyable years.

Abstract

The motion of a single elongated (Taylor) bubble propagating in a transparent vertical pipe is studied experimentally in stagnant liquid, as well as in upward and downward liquid flow. Digital image processing of a sequence of video images serves as the main experimental method for the study of the Taylor bubble motion. In addition, the distribution of the velocities in front of the bubble and in the liquid film is measured using Particle Image Velocimetry. The relation between the Taylor bubble motion and the velocity field in front of it is discussed.

Keywords: Two-phase slug flow; Image processing; PIV

1. Introduction

The flow of gas and liquid in pipes can occur in a number of configurations termed flow patterns. One of the most complicated flow patterns is the slug flow. It occurs over a wide range of parameters, for all pipe inclinations and for a wide range of gas and liquid flow rates.

* Corresponding author. Tel.: +972-3-640-8504; fax: +972-3-640-7334.
E-mail address: dbarnea@eng.tau.ac.il (D. Barnea)

0301-9322/99/$ - see front matter
PII: S0301-9322(99)00037-3

Slug flow is characterized by a quasi-periodic alteration of long bullet-shaped bubbles and liquid slugs.

In vertical pipes, elongated (Taylor) bubbles are axisymmetrical and have a round cup, while the tail is generally assumed to be nearly flat. The liquid around the elongated bubbles moves downstream as a thin falling film. The liquid velocity in the film is substantially larger than the mean velocity in the liquid slug ahead of the bubble. Each slug sheds liquid in its back to the subsequent film, which accelerates as it moves downward. Then it is injected into the next liquid slug as a circular wall jet, producing a mixing zone in the bubble wake. The mixing zone is generally believed to have a shape of a toroidal vortex. The flow gradually reestablishes in the body of the liquid slug behind the mixing zone.

In the case of downward flow of liquid in a vertical pipe (Griffith and Wallis, 1961; Nicklin et al., 1962; Martin, 1976), the bubble shape can be asymmetrical. The tip of the bubble is inclined to the pipe wall to avoid the fast-moving liquid in the pipe center. If the liquid flow rate is high enough, the bubble may remain stationary or even descend instead of rising.

The motion of a single elongated bubble in a vertical pipe is closely related to the movement of Taylor bubbles in slug flow. The translational velocity of the elongated bubble, U_t, is affected by two factors: the velocity of the liquid ahead of the bubble cap U_L, and the buoyancy-induced velocity of the bubble in stagnant liquid, i.e., the drift velocity of the bubble, U_0.

Numerous researchers have studied the motion of a single elongated bubble in stagnant liquid analytically and experimentally. Usually, the asymptotic cases are considered: inertial flow, viscous flow and capillary flow. The ranges of these regimes were determined experimentally by White and Beardmore (1962).

The drift velocity is determined by the three-dimensional flow at the front of the bubble. For the case of inertial flow (where both interfacial and viscous effects are negligible) the fluid is assumed to be inviscid. Dumitrescu (1943) and Davies and Taylor (1950) performed an analysis based on potential flow for the vertical case and obtained the following expression for the drift velocity:

$$U_0 = k\sqrt{gD}. \tag{1}$$

Dumitrescu (1943) found that the value of the coefficient k in Eq. (1) is equal to 0.351, while Davies and Taylor (1950), who used a less accurate solution, obtained $k = 0.328$. Measurements show that the value of k is in the range of 0.33–0.36 (Nicklin et al., 1962; Goldsmith and Mason, 1962; Clift et al., 1978).

A theoretical analysis for calculating the drift velocity in horizontal pipes was presented by Benjamin (1968). His analysis is based on the assumption that the bubble drift velocity is the same as the velocity of the penetration of a cavity when the liquid is drained from a horizontal pipe opened from one end. Benjamin obtained the value of $k = 0.542$ for the horizontal case. Alves et al. (1993) extended Benjamin's approach to the inclined and vertical cases, taking into consideration surface tension effects. Experimental studies on the drift velocity in inclined pipes as well as in vertical and horizontal pipes were performed by Singh and Griffith (1970), Bonnecaze et al. (1971), and Bendiksen (1984).

For a Taylor bubble rising in a moving liquid, Nicklin et al. (1962) suggested that the

translational velocity of the bubble is a superposition of its rise velocity in stagnant liquid U_0 and the contribution due to the mean liquid velocity U_L:

$$U_t = CU_L + U_0. \tag{2}$$

They also measured the velocity of the bubble nose in stagnant liquid under different cases of hydrostatic expansion; i.e. when liquid is removed below or above the bubble. If the bubble is allowed to expand downward, the velocity of the bubble nose remains the same as the bubble rise velocity in a pressurized tube. When the bubble expands upward, its velocity increases linearly, and the rate of acceleration is related to the pressure gradient. In this case, the coefficient C in Eq. (2) was found to be not zero but 1.48, in spite of the fact that the liquid was initially at rest.

Griffith and Wallis (1959) showed that for continuous slug flow, the liquid velocity U_L in Eq. (2) should be replaced by the mixture velocity:

$$U_t = CU_M + U_0, \tag{3}$$

where $U_M = U_{LS} + U_{GS}$ is the total mixture velocity, U_{LS} and U_{GS} are the liquid and gas superficial velocities, respectively.

The value of the factor C in Eq. (2) depends on the velocity profile in the liquid ahead of the bubble, and can be seen as the ratio of the maximum to the mean velocity in the profile. Hence, for turbulent flows, $C \cong 1.2$, while for laminar pipe flow, $C \cong 2$ (Nicklin et al., 1962; Collins et al., 1978; Grace and Clift, 1979; Bendiksen, 1985). Shemer and Barnea (1987) performed a visualization of the velocity profiles behind Taylor bubbles in vertical and horizontal slug flows. They found that the tip of the trailing bubble in the wake of the leading one follows the location of the maximum instantaneous velocity in the wake.

Tung and Parlange (1976) and Bendiksen (1985) analyzed the influence of surface tension on the bubble velocity in the inertial regime, first in stagnant liquid and then in upward flow. Surface tension was found to decrease the bubble velocity, up to a stationary bubble if surface tension is high enough. However, in most practical applications surface tension is negligible.

So far the effect of the flow field ahead of the Taylor bubble on its motion was considered. The reverse problem of the effect of the bubble motion on the flow field around the Taylor bubble obtained considerably less attention.

Goldsmith and Mason (1962) made an attempt to measure the velocity profiles directly in front of the bubble and in the liquid film by tracing of aluminum particle displacements in still photographs of the flow. The inception of the reverse flow in the liquid film was observed. The results agreed well with their model.

Kvernvold et al. (1984) used LDV-technique for measuring the velocity profiles at a limited number of cross-sections in the slug and in the liquid film in horizontal slug flow. Nakoryakov et al. (1986,1989) performed a more extensive study of the instantaneous velocity field and shear stresses in vertical slug flow by means of an electrochemical velocity probe. Radial and axial velocity profiles were obtained. Mao and Dukler (1989) measured the distribution of the wall shear stress in vertical slug flow. They demonstrated a double change in the flow direction in a slug unit: close to the bubble nose where the film formation begins; and in the beginning

of the liquid slug where the mixing zone ends. The axial locations of the onset and termination of the reverse flow were close to those measured by Nakoryakov et al. (1986,1989).

DeJesus et al. (1995), Kawaji et al. (1997) and Ahmad et al. (1998) applied the photochromic dye activation method to measure the flow field around a bubble rising in stagnant liquid (kerosene). The instantaneous velocity distributions in front of the bubble, in the liquid film and in the near wake were visualized. In addition, averaged velocity profiles in the liquid film were presented. Mao and Dukler (1990,1991) performed numerical simulations to calculate the velocity field in front of the bubble and in the liquid film. Clarke and Issa (1992,1993) and Bugg et al. (1998) calculated the complete flow field around a bubble rising in stagnant liquid.

Gas–liquid slug flow is characterized by the presence of a clearly seen moving interface. This feature makes the flow visualization methods an obvious choice for the measurement technique. Tassin and Nikitopolous (1995), Lunde and Perkins (1995) and Donevski et al. (1995) proposed methods based on video imaging and digital image processing for measuring shape, size and velocity of bubbles in a large volume of liquid. Polonsky et al. (1999) applied this technique to obtain detailed quantitative data on the instantaneous characteristics of the bubble motion.

The purpose of the present study is to use the image processing technique, including PIV, in order to investigate the mutual relation between a single rising bubble and the flow field around it. This research is aimed at investigating the effect of the flow field ahead of the bubble on the translational velocity of the bubble and the effect of the bubble motion on the liquid velocity field.

2. Experimental system and methods

The test section (Fig. 1) is made of a vertical transparent Perspex pipe, 25 mm in diameter and about 4 m (170 diameters) long. It consists of three interchangeable visualization sections (each about 1 m long) connected by flanges, and 1 m long initial section. Each of the visualization sections is equipped with a separate rectangular transparent box filled with water, in order to reduce image distortion and to provide cooling against illumination heat. There is still some residual image distortion due to the small difference in the refraction coefficient of the wall material ($n = 1.5$) and water ($n = 1.33$). Filtered tap water flowing in a closed loop is used as the working fluid. The air supply system consists of an inlet air chamber and three electrically activated valves: an injection valve, a drainage valve and a blowing valve. Air is supplied from a central compressed air line at a nominal pressure of 0.6 MPa. The 1 m long air inlet chamber is attached to the lower part of the test pipe at an angle of 30°. Individual bubbles are injected from this chamber, which is connected to the test pipe by a computer-controlled injection valve. The valve, the chamber and the test section have the same inner diameter, in order to provide a smooth entrance of air bubbles. The length of the injected bubbles is determined by the duration of the valve opening, which is controlled by the computer, as well as by the accurately monitored air pressure in the chamber.

Two experimental techniques are used. The digital image processing is employed for the measurements of the instantaneous and time-averaged parameters of the bubble moving along the pipe, such as its propagation velocity and shape, while the Particle Image Velocimetry

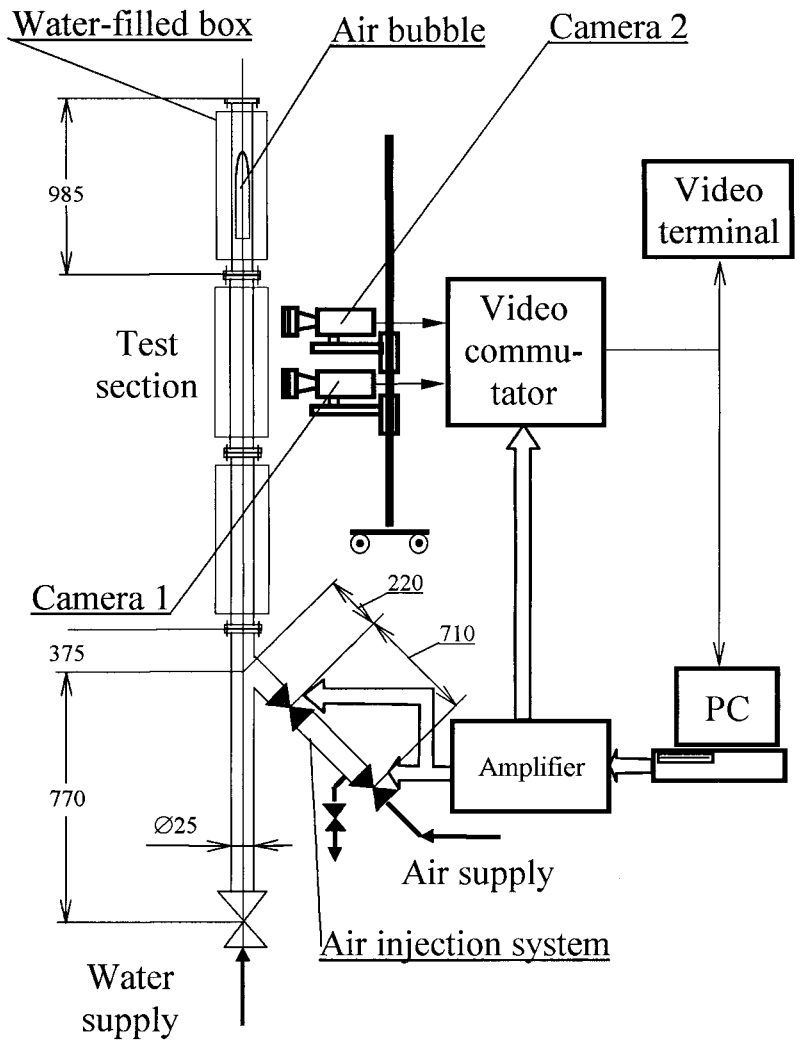

Fig. 1. Experimental facility.

(PIV) technique provides the flow field in the liquid surrounding the bubble. A detailed description of the digital image processing algorithm is given in Polonsky et al. (1999).

Two interlaced black-and-white NTSC synchronized video cameras are used for the measurements of the bubble propagation velocity along the pipe. In these measurements, illumination is provided by a set of 500 W halogen lamps. In the measurements of the bubble shape and the film thickness, as well as in the PIV measurements, a single camera located close to the test section is used. Illumination of the field of view is provided in this case by a 5 W Argon ion laser light sheet about 50 mm high and 1 mm thick.

The PIV is a non-intrusive method that provides both qualitative visualization and quantitative measurements of the two-dimensional velocity field (see, e.g., Adrian, 1991). Separation of the odd and even fields of the interlaced frame produces two non-interlaced

images with a time interval of 1/60 s between them. A small amount (about 0.1‰) of almost neutrally buoyant (density 0.95) polystirol spheres 20–40 μm in diameter is added to the water in the PIV experiments. The particles contain fluorescent dye and emit light in the yellow-orange region of the spectrum when illuminated by the laser. Therefore, a yellow filter is put on the camera objective lens, so that the light sheet itself is filtered out from the images and only the particles are seen as bright speckles. Double exposure that is necessary for the velocity measurements is achieved by the use of image interlacing (see Polonsky (1998) for further details). For the measurements of the flow velocity in the film, which is significantly higher than the translational velocity of the bubble, a streak length method is implemented. The configuration of the system is similar to that employed in the PIV measurements, but the camera shutter is kept completely open, so that in each frame the particles produce streaks whose lengths are proportional to the liquid velocity.

The output video signals are digitized at the rate of 30 fps and stored directly in the RAM of a personal computer and then transferred to a hard disk for permanent storage. The clock of the PC provides the necessary synchronization between the various devices, i.e., the bubble injection, the switching between the cameras, and the recording process.

3. Experimental results

3.1. Translational velocity of the Taylor bubble

The translational velocity of the Taylor bubble U_t can be measured from the displacement of the bubble nose. The averaged results for the bubble translational velocity are obtained for each liquid flow rate using a sequence of 100 to 200 recorded images of individual bubbles. The effect of the bubble length on U_t was studied in Polonsky et al. (1999) and was found to be relatively weak. This effect is attributed to the bubble expansion while rising along the unpressurized pipe. The bubble expansion results in a displacement of the liquid ahead of the bubble thus causing an additional contribution to the liquid velocity ahead of the bubble. As a result of that, the longer is the bubble, the faster is its rising velocity.

The drift velocity U_0 can be determined from the measured translational velocity in stagnant liquid in the limit of short bubbles, where the effect of compressibility vanishes (see Polonsky et al., 1999). This value is found to be $U_0 = 17.4$ cm/s, corresponding to $k = 0.351$. This result is close to the value of $k = 0.35$ which is usually used in the calculations of the drift velocity in an inertial regime (Dumitrescu, 1943; Nicklin et al., 1962). It should be remembered that the value $k = 0.35$ is by no means exact. The value obtained in the present experiments lies well within the range of k reported by different researchers for an air–water system: 0.346 by Davies and Taylor (1950), 0.33–0.38 by Goldsmith and Mason (1962) and 0.33–0.36 by Clift et al. (1978).

Applying Eq. (2) for non-zero liquid flow rates with $U_0 = 17.4$ cm/s allows one to calculate the coefficient C from the measured values of the bubble translational velocity U_t. Liquid velocities in the range -14 cm/s $< U_L <$ 25.5 cm/s are studied (the minus sign denotes downward velocities). The maximum value of the Reynolds number based on the liquid velocity, $Re_L = U_L D/\nu_L$, is thus 6380. Flow visualization indicates that for all liquid flow rates

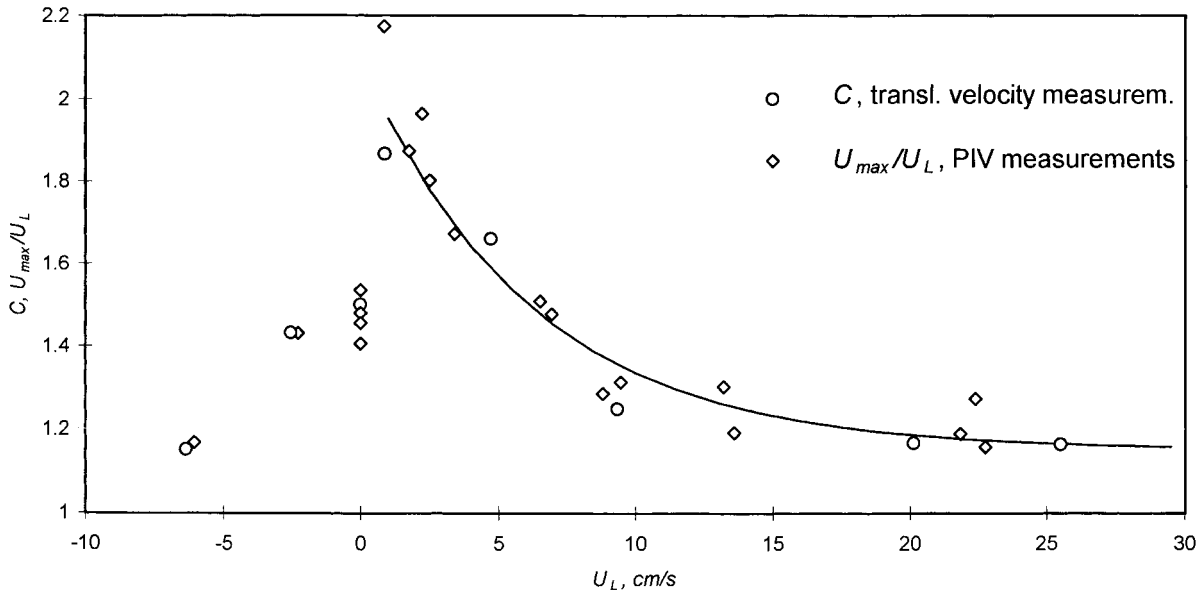

Fig. 2. The relation between C and the velocity profiles ahead of the bubble.

employed here, the flow remains laminar. The dependence of the coefficient C on U_L as obtained in the present measurements is shown in Fig. 2. As expected, the values of C are found to depend on the liquid flow velocity. For upward flow, the coefficient C decreases from about 1.9 at very low liquid flow rates, to about 1.2 for the highest flow rates. Note that for longer Taylor bubbles, gas expansion due to compressibility results in an induced liquid velocity in front of the bubble. For stagnant water, the replacement of U_L in Eq. (2) by this induced velocity yields the coefficient $C = 1.5$.

The assumption that the coefficient C in Eq. (2) is determined by the maximum liquid velocity ahead of the bubble is verified here by measuring the velocity profiles in front of the Taylor bubble. The velocity profiles are measured at a distance exceeding $10D$, where the presence of the bubble does not affect the liquid velocity field, as will be shown in sequel. The velocities are measured by means of PIV technique. The resulting velocity profiles are presented in Fig. 3(a)–(c) for stagnant, up flowing and down flowing liquid, respectively. Each profile in Fig. 3 represents an average of about 80 to 160 individual PIV measurements at each particular axial and radial location. Error bars, representing the root mean square (rms) standard deviation, are given in Fig. 3(a) only. The relative error is usually within the range of $\pm 10\%$. Similar relative errors are obtained in the measurements represented in Fig. 3(b) and (c). The error bars are not plotted in those figures for sake of clarity.

The measured velocities in stagnant liquid, Fig. 3(a), are quite small, 1–6 mm/s, and increase linearly with the bubble length. The contribution of the velocity induced by the bubble expansion can thus be ignored for non-zero liquid flow rates. Note that the velocity profiles in Fig. 3(a) are not yet completely developed. The ratio of the maximum to the average velocity

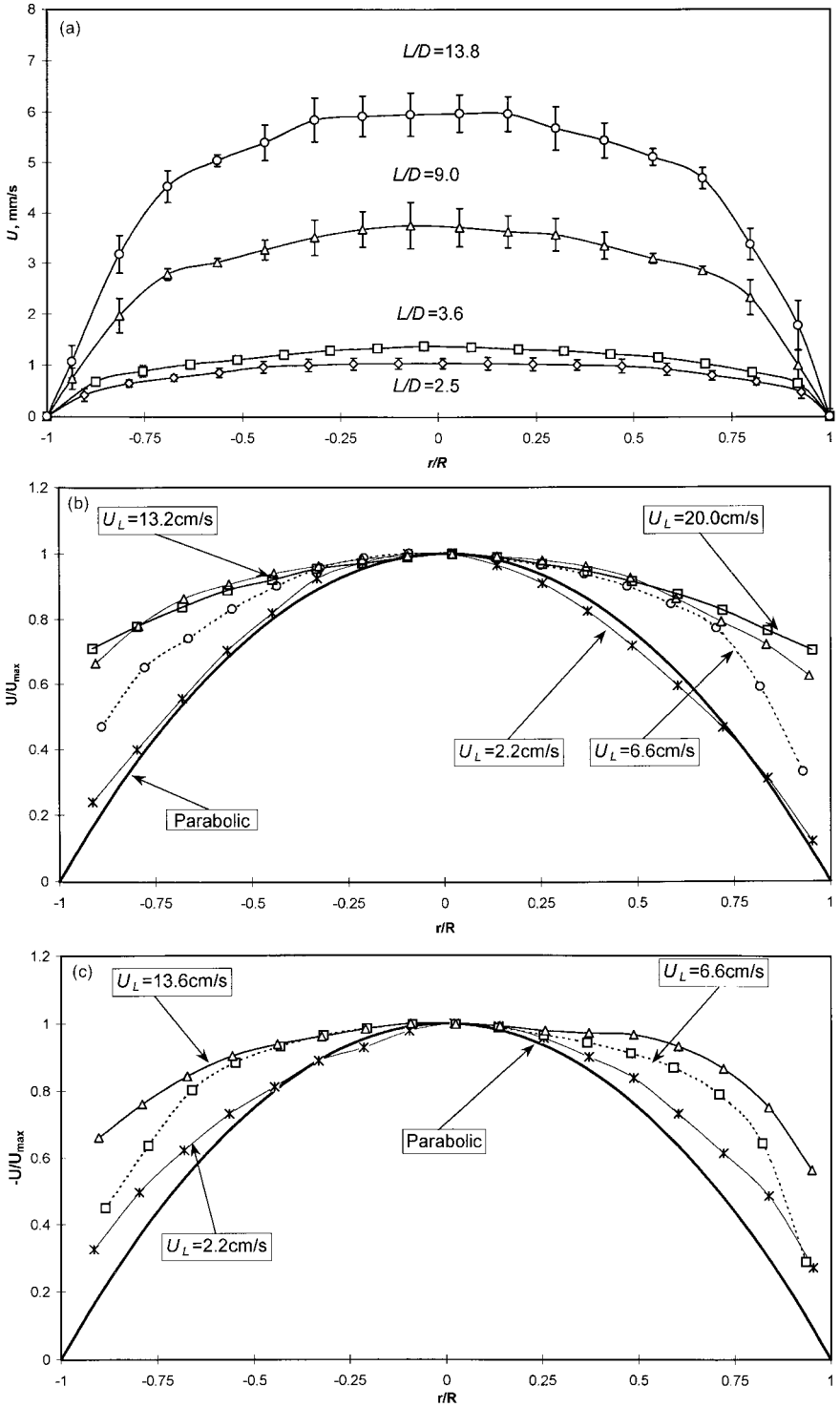

Fig. 3. (a) Induced velocity profiles in stagnant water due to bubble expansion. (b) Velocity profiles ahead of the bubbles in upward flow. (c) Velocity profiles ahead of the bubble in downward flow.

determined from the velocity profiles in Fig. 3(a) is also shown in Fig. 2. No dependence of this ratio on the bubble length is found and the average value is about 1.47. This value is close to the value of $C = 1.5$ which is calculated from the translational velocity data, see Fig. 2, and also to the result of $C = 1.48$ obtained by Nicklin et al. (1962).

The velocity profiles in Fig. 3(b) and (c) are normalized by the maximum velocity U_{max}. The theoretical parabolic velocity profile in laminar flow is plotted together with the experimental results. For up-flowing liquid, the laminar velocity profiles in Fig. 3(b) are relatively flat, since the flow at the measuring location, which is 2.5 m from the entrance to the pipe, is still undeveloped. The ratio of the maximum to the averaged velocity calculated from the measured profiles is plotted in Fig. 2. The results of Fig. 2 clearly indicate that this ratio is indeed very close to the values of the coefficient C obtained from the measurements of the Taylor bubble translational velocity. Note that although the flow is laminar for all flow rates examined in this study, the values of the ratio of the maximum and the mean velocity in the cross-section, as well as those of C, are lower than 2 and decrease with U_L. This is due to the fact that the entrance length increases with Re_L, and thus at the measurement location the profiles for higher flow rates are less developed. Therefore, for low values of Re_L, and correspondingly short entrance regions, the value of the coefficient C in Eq. (2) indeed approaches 2.

For relatively slow downward flow, the propagation direction of the bubble (upward) is opposite to that of the flowing liquid. The liquid velocity is negative everywhere except at the wall where it vanishes. Thus, the maximum velocity ahead of the rising bubble in downward flow is attained at the pipe wall. This can explain the observed tilting of the Taylor bubble tip towards the pipe wall in downward flow, while in upward and in stagnant liquid the rising bubble retains axial symmetry, see Fig. 4. This asymmetry increases with increasing downward liquid velocity. Surface tension apparently prevents the shifting of the bubble tip to locations very close to the wall. Based on these considerations, for the downward case the value of U_{max} in Fig. 2 is replaced by the liquid velocity in the averaged velocity profile ahead of the bubble taken at the location of the bubble tip, $U(R_{tip})$.

Note that in our experiments, the measurement station is situated at a distance of 1.4 m from the upper end of the pipe. Contrary to the case of up-flowing liquid, where not only the averaged but also the instantaneous velocity profiles exhibit axial symmetry, in downward flow only the averaged profiles plotted in Fig. 3(c) are symmetric, while the instantaneous velocity distributions are unsteady and asymmetric, with the maximum displaced from the pipe axis. This flow unsteadiness causes oscillations of the bubble tip from one side of the pipe to the other.

The results of Fig. 2 demonstrate that the values of the coefficient C determined from the measurements of the bubble translational velocity agree well with the ratio of the local liquid velocity ahead of the tip of the Taylor bubble, $U(R_{tip})$, to the mean liquid velocity U_L. For upward flow, $U(R_{tip})$ corresponds to the maximum liquid velocity, U_{max}, at the center-line of the pipe. For down flow, the location of the bubble tip R_{tip} is determined by the tendency of the bubble tip to move towards the pipe wall and by the surface tension effects. Eq. (2) thus can be modified and written as

$$U_t = U\left(R_{tip}\right) + U_0. \tag{4}$$

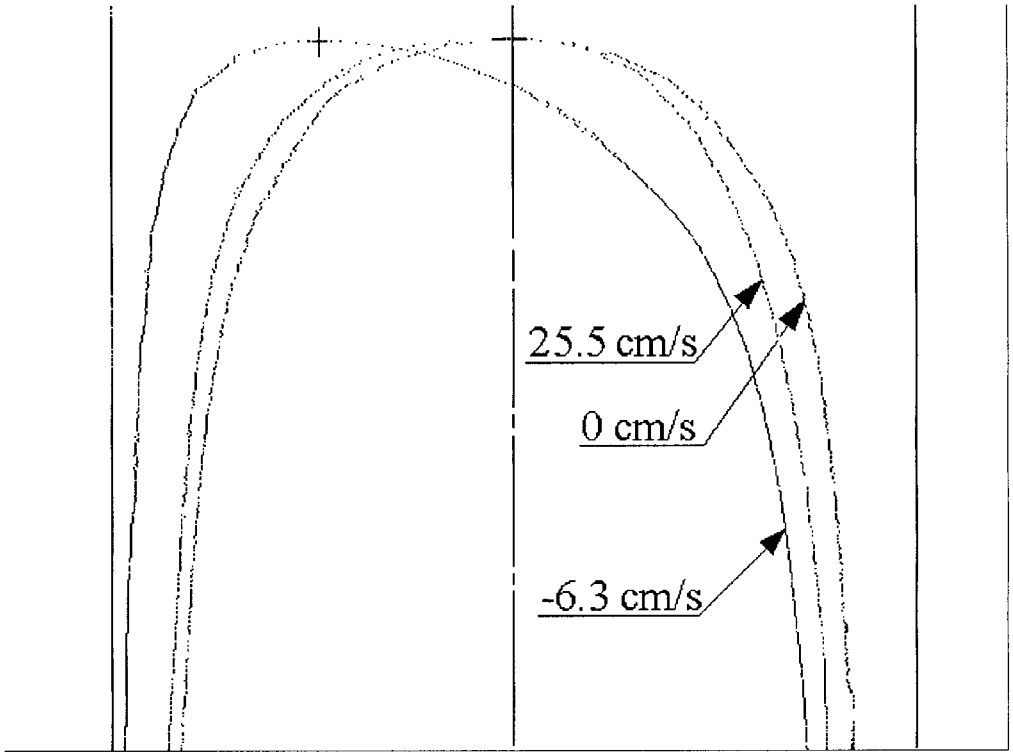

Fig. 4. Instantaneous bubble nose shape for various liquid velocities.

3.2. Flow field in front of a rising bubble

The velocity distribution far ahead of the bubble, discussed so far, determines the influence of the liquid motion on the Taylor bubble velocity, i.e. the contribution of the term CU_L to the bubble translational velocity in Eq. (2). We now proceed to the measurements of the velocity field in the near vicinity of the bubble, which determines the drift velocity U_0. The measurements are performed for stagnant liquid and upward liquid flow. In each test run, a short sequence of PIV images is acquired. The number of frames in a sequence varies from 4 to 12 depending on the bubble translational velocity, and the velocity field is calculated for each image in sequence. The PIV processing is performed over an interrogation region of the size of about 3 mm by 3 mm (the corresponding linear number of pixels range from about 30 to 75). The size of the interrogation region puts a limit on the spatial resolution of the PIV measurements. The obtained velocity fields are shifted in the vertical direction by a number of pixels that is equal to the shift of the bubble nose between two successive images. This operation fixes their position relative to the bubble tip. Note that the velocities are presented in a frame of reference fixed relative to the pipe wall, however the averaging of the instantaneous velocities is performed at locations that are fixed relative to the moving bubble.

Successive two-dimensional velocity fields in front of the bubble in stagnant liquid are shown in Fig. 5. The bubble outline is shown as well. In the PIV technique each velocity field is calculated from two successive images, the time interval between the images in our case is 1/60 s, so that the bubble shift between consecutive images is about 3 mm. The positions of the bubble shown in Fig. 5(f)–(h) correspond to the average between two images used for the calculation of the velocity field. Along the pipe axis, the flow accelerates from nearly zero velocity far away from the bubble up to $U_0 = 17.4$ cm/s at the bubble interface. Away from the pipe axis, a flow in the radial direction is clearly seen, which gradually develops into a reversed flow at the walls and then into a liquid film around the bubble.

It is clearly seen in Fig. 5 that the flow is almost symmetrical, which permits the averaging of the left and right sides of the velocity profile. The radial distribution of the axial velocity component V_x in front of the bubble, averaged over the left and right sides of the pipe, is shown in Fig. 6(a). The distance is given relative to the average position of the bubble tip between two consecutive images. The profiles shown start from 28 mm ($1.13D$) ahead the bubble, where the liquid is essentially undisturbed (except for the expansion-induced velocity, which is $U_L = 0.12$ cm/s for the case of a $4D$ long bubble) up to a distance of 3 mm from the bubble tip. The minimal distance from the bubble where the velocity can be measured is determined by the spatial resolution of the present measurements. The onset of the reverse flow is detected at a distance of about 16 mm ($0.66D$) in front of the bubble. This result agrees with the observation of DeJesus et al. (1995), who reported on the presence of a very slow downward flow at a distance of 0.5 cm ($0.2D$) ahead of the bubble.

The radial distribution of the radial velocity component V_r is shown in Fig. 6(b). The radial velocity increases with the approach to the bubble, as the rising bubble pushes the liquid aside. When the film around the bubble is formed, a decrease in the radial velocity occurs, as the flow in the liquid film becomes essentially one-dimensional.

Measurements are also performed in front of a bubble rising in upward flowing liquid. The PIV measurements of the 2D-velocity field yield results that are qualitatively similar to those presented in Fig. 5 and indicate that the velocity profiles in upward flow are symmetrical. The absolute values of the velocities are higher than those measured in stagnant liquid. The maximum velocity limit of the adopted PIV technique, which is based on picture interlacing, prevents measurements in the close vicinity of the bubble. Detailed results of these measurements are given in Polonsky (1998).

An example of the averaged radial distributions of the axial velocity in the pipe cross-section in front of a $5D$ long bubble is shown in Fig. 7 for the upward liquid velocity of $U_L = 0.9$ cm/s. The inception of the reverse flow at the periphery of the pipe occurs here closer to the bubble than in stagnant water. The negative axial velocity is detected at a cross-section located at about $x = 6$ mm in front of the bubble. For higher liquid flow rates, negative velocities are detected closer to the bubble tip. For example, for $U_L = 6.2$ cm/s, negative velocities are detected at 1 mm in front of the bubble. The same trend was found by Nakoryakov et al. (1989) and Mao and Dukler (1989) who studied slug flow at high velocities of liquid and gas. They observed the onset of the reverse flow at a short distance down from the bubble tip, the reverse point is moving down as the mixture velocity increases.

Fig. 8 summarizes the data on the variation of the maximum liquid velocity along the pipe axis as a function of the distance from the bubble tip, for different liquid velocities and for

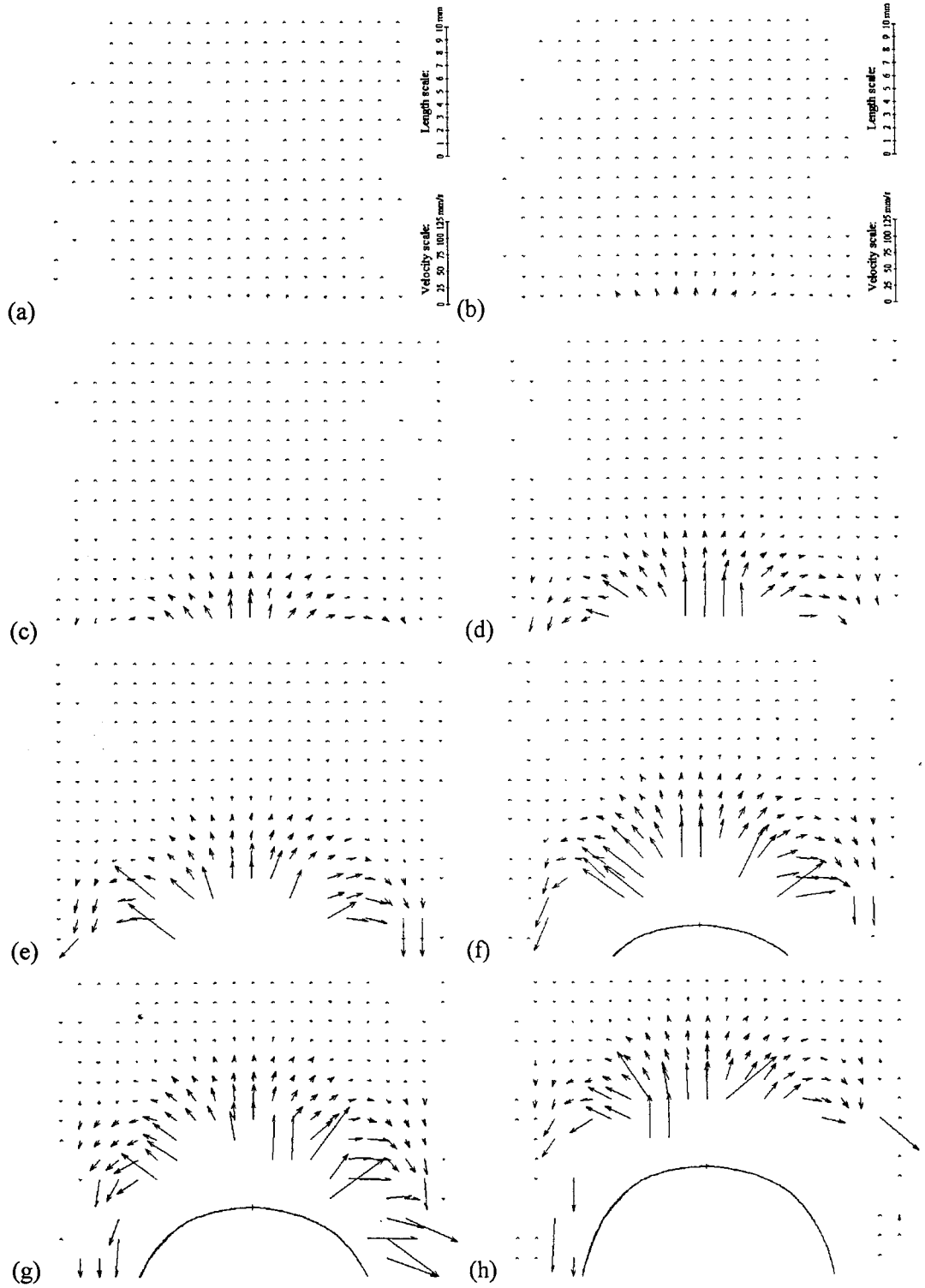

Fig. 5. Sequence of velocity fields in front of the 4*D* bubble in stagnant liquid. The time increment between consecutive images is 1/60 s.

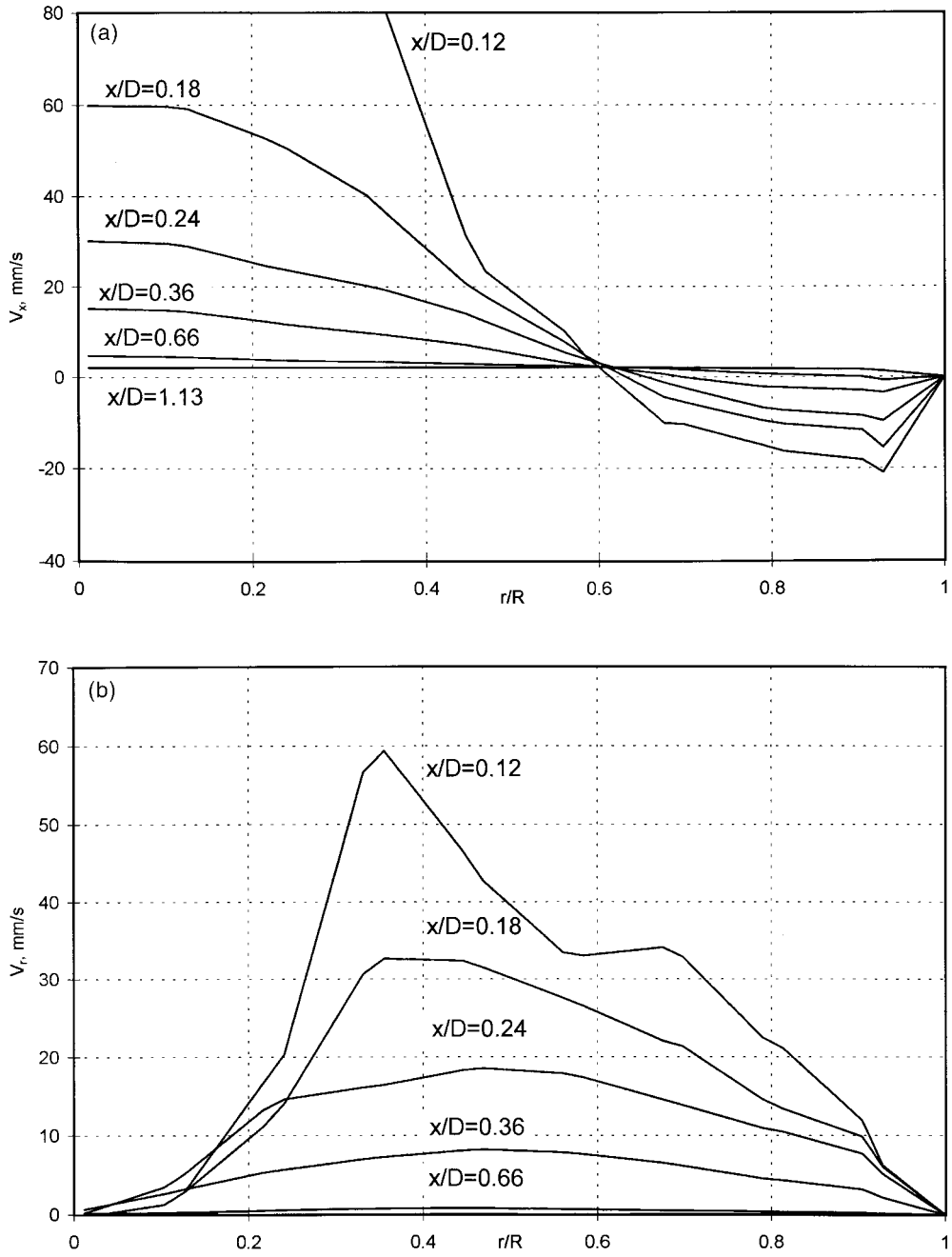

Fig. 6. Velocity profiles in front of a 4*D* bubble in stagnant liquid at various distances from the bubble tip. (a) Axial velocity component. (b) Radial velocity component.

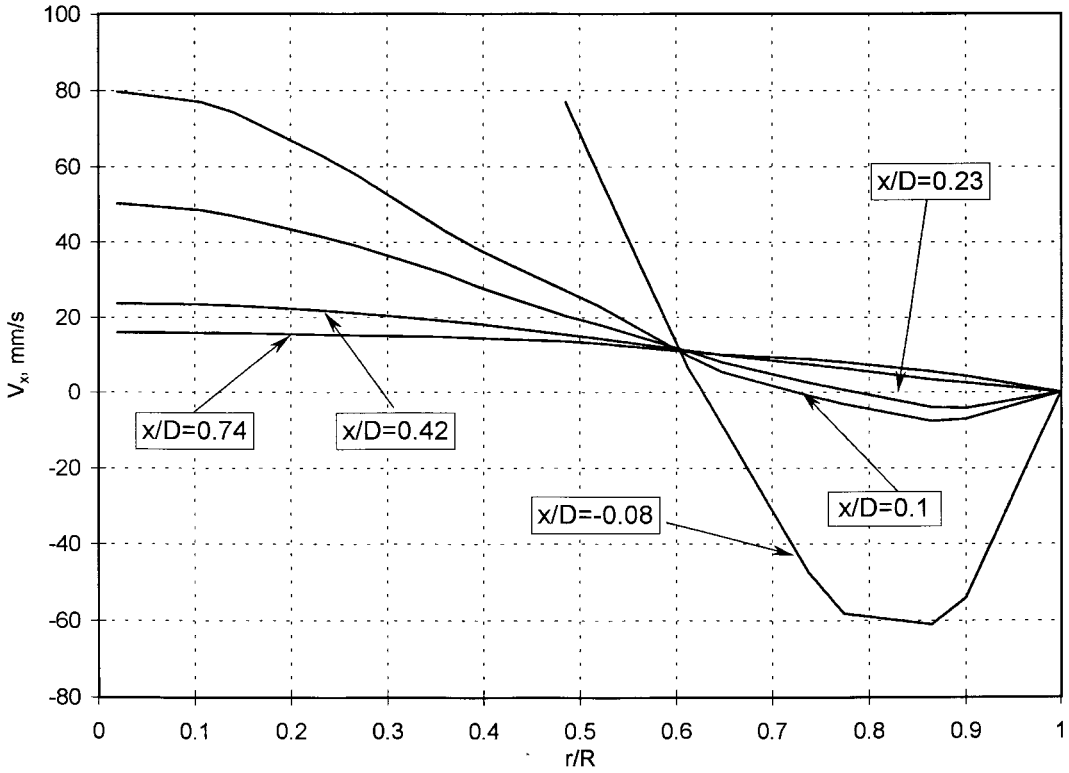

Fig. 7. Axial velocity profiles at various distances ahead of a $5D$ long bubble, $U_L = 0.9$ cm/s.

bubbles of similar length. The liquid velocity at the point $x = 0$, which corresponds to that of the bubble interface, is equal to the translational velocity of the bubble nose as obtained from the bubble propagation velocity measurements (see Polonsky et al., 1999). The lines represent the best fit of the experimental data. This figure demonstrates that the influence of the bubble is detectable in the liquid only at distances closer than about $1D$ from the bubble tip. The flow ahead of this point is essentially undisturbed by the bubble presence. In their numerical simulations Mao and Dukler (1991) obtained that the velocity of the liquid is influenced by the presence of the bubble at distances exceeding 2 m ($80D$) for a liquid flow rate of 0.29 m/s ($Re_L = 14{,}500$). This discrepancy may stem from the different flow conditions (turbulent slug flow modeled by Mao and Dukler and laminar flow in the present experiments).

3.3. Velocity of the liquid in the film

The velocity of the liquid film is significantly higher than the translational velocity of the bubble, which is evident from the continuity equation. During the time interval of 1/60 s between two half-frames of the interlaced video signal, the shift of the particles in the image may be quite large (tens of pixels). Hence, PIV measurements of the film velocity based on

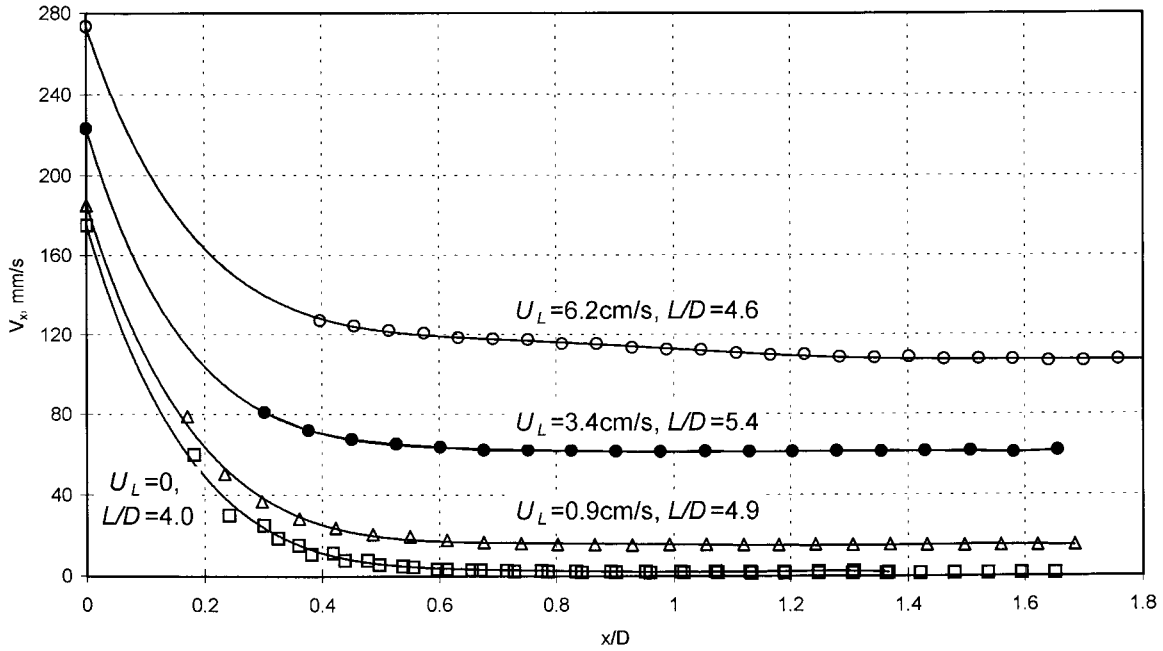

Fig. 8. Variation of the axial velocity along the pipe axis.

image interlacing cannot be implemented. The particle streaks technique is therefore used for the measurements of the liquid velocity in the film. In these experiments, the camera shutter is completely open for the whole duration of each half-frame of 1/60 s, so that the particles produce long streaks whose length is proportional to the local liquid velocity.

Radial distributions of the measured instantaneous axial velocity component at several axial locations relative to the bubble tip are presented in Fig. 9. Note that the horizontal resolution in the corresponding video images is about 20 pixel/mm. It should be stressed that in spite of the fact that the flow in the liquid film is basically one-dimensional, the particles may occasionally leave the illuminated laser sheet while the shutter is open. This effect, as well as some image distortion due to small mismatch in the refraction indices of Perspex and water, may contribute to the scatter in the film velocity data in Fig. 9. The solid lines in this figure represent the best fit of the experimental data assuming a parabolic velocity profile in the film with zero velocity at the pipe wall and zero shear stress at the gas–liquid interface (Meisen and Boersman, 1995).

As required by mass conservation, the film velocity increases as the film thickness decreases along the bubble. The Reynolds number calculated on the basis of film thickness and average film velocity increases from $Re_f = 0$ at $x/D = 0$ at the bubble tip to $Re_f = 1000$ at $x/D = 6.4$, so that the flow in the film remains laminar. The velocity profiles are flatter than the theoretical parabolic profiles, which suggests that the flow in the film remains undeveloped at the axial locations of the present experiments (up to $6.4D$). These results agree with the measurements of Kvernvold et al. (1984) by means of LDA, as well as with the observations of

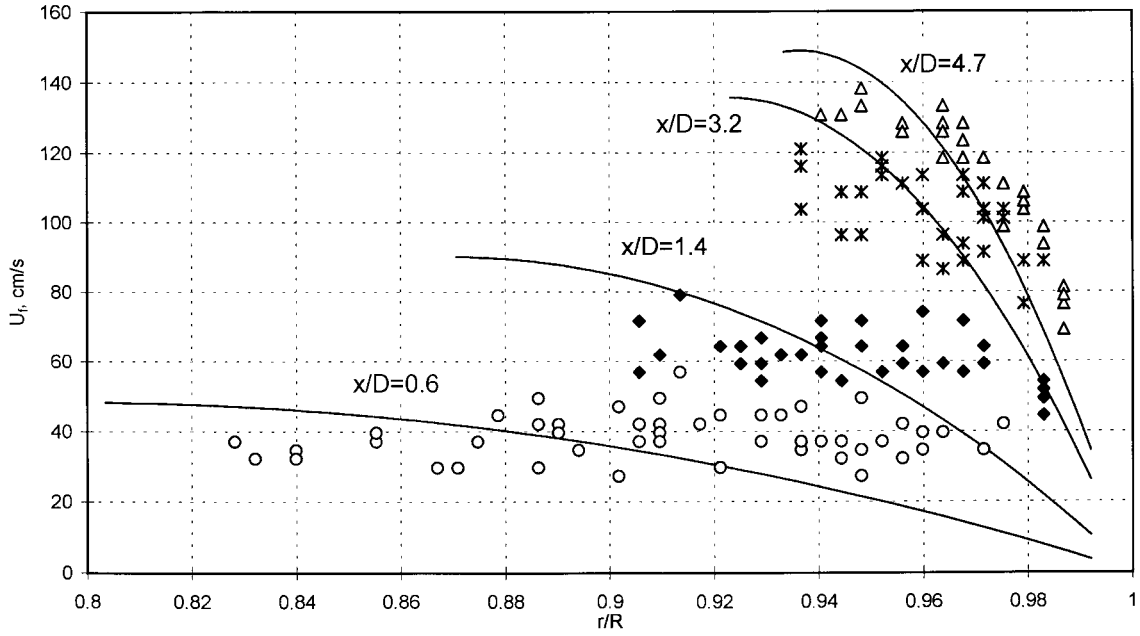

Fig. 9. Radial distributions of the velocity in the liquid film as a function of the distance from the bubble tip.

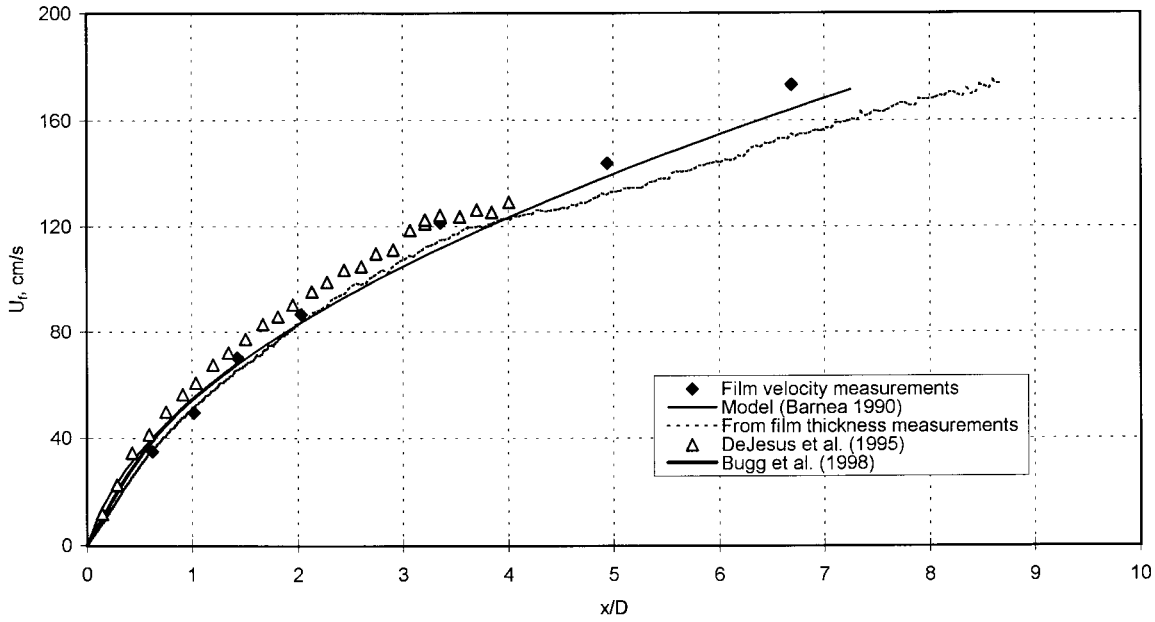

Fig. 10. Average velocity in the liquid film as a function of the distance from the bubble tip.

DeJesus et al. (1995) and Kawaji et al. (1997) who used the photochromic dye activation method.

Fig. 10 presents the axial distribution of the average velocity in the film. The present experimental results denoted by diamonds are obtained by integration of the best-fit curves from Fig. 9. The solid line gives the theoretical results according to Barnea (1990), while the broken line is the calculated film velocity from the experimentally measured film thickness (Polonsky et al., 1999) together with a mass balance in the film. The results show reasonable agreement between the average film velocities obtained by the different methods. The average film velocities are also in a very good agreement with the measurements of DeJesus et al. (1995) and with the numerical simulation of Bugg et al. (1998).

4. Summary and conclusions

Investigation of the hydrodynamic parameters of a single elongated (Taylor) bubble moving in a vertical pipe is performed. Simultaneous application of the digital image processing and the PIV technique makes it possible to extract new information on the Taylor bubble motion. The flow field ahead of the bubble, as well as the velocity profiles in the film that surrounds the bubble are measured. The relation between the Taylor bubble propagation velocity and the flow field ahead of it is analyzed. These characteristics are very important for the appropriate modeling of developed and transient slug flow.

It is usually assumed that the propagation velocity of the bubble is related to the maximum local liquid velocity ahead of it. This assumption is confirmed here by direct measurements of the cross-sectional velocity profiles by PIV. The factor C is found to be very close to the ratio of the maximum to the average velocity in the profile, U_{max}/U_L.

The measurements of the liquid velocity profiles in the present study are performed at a fixed axial location. Since the length of the entrance region in the pipe is a strong function of the Reynolds number, the liquid velocity profiles for different liquid flow rates are obtained at varying effective distances from the pipe inlet, and thus exhibit varying values of the ratio U_{max}/U_L. It should be stressed here that in a real developed or transient slug flow, the liquid slug length is often shorter than the entrance length necessary for attaining a fully developed velocity profile. The results of the present study thus can be used for modeling such flows.

The effect of the rising bubble on the liquid velocity field ahead of it is restricted to distances of about $1D$ from the bubble tip, except for the additional liquid flow rate induced by the bubble hydrostatic expansion. In the present experiments, the inception of negative velocity is observed in front of the Taylor bubble tip. The location of the onset of the reversed flow is found to be dependent on the liquid flow rate. As the liquid velocity increases, the point of flow reversal moves down. These results agree with those reported elsewhere for significantly higher liquid flow rates, where the onset of the reverse flow was observed downstream in the liquid film.

The local velocity in the liquid film is measured by means of a particle tracking method. The measured velocity profiles are found to be undeveloped, and almost flat. The average film velocities are in agreement with the model of Barnea (1990), as well as with other available experimental and numerical results.

References

Adrian, R.J., 1991. Particle-imaging techniques for experimental fluid mechanics. Annu. Rev. Fluid Mech. 23, 262–304.

Ahmad, W.R., DeJesus, J.M., Kawaji, M., 1998. Falling film hydrodynamics in slug flow. Chem. Eng. Sci. 53, 123–130.

Alves, I.N., Shoham, O., Taitel, Y., 1993. Drift velocity of elongated bubbles in inclined pipes. Chem. Eng. Sci. 48, 3063–3070.

Barnea, D., 1990. Effect of bubble shape on pressure drop calculations in vertical slug flow. Int. J. Multiphase Flow 16, 79–89.

Bendiksen, K., 1984. An experimental investigation of the motion of long bubbles in inclined tubes. Int. J. Multiphase Flow 10, 467–483.

Bendiksen, K., 1985. On the motion of long bubbles in vertical tubes. Int. J. Multiphase Flow 11, 797–812.

Benjamin, T.B., 1968. Gravity currents and related phenomena. J. Fluid Mech. 21, 209–248.

Bugg, J.D., Mack, K., Rezkallah, K.S., 1998. A numerical model of Taylor bubbles rising through stagnant liquid in vertical tubes. Int. J. Multiphase Flow 24, 271–281.

Bonnecaze, R.H., Eriskine Jr., W., Greskovich, E.J., 1971. Holdup and pressure drop for two-phase slug flow in inclined pipelines. AIChE J. 17, 1109–1113.

Clarke, A., Issa, R.I., 1992. A multidimensional computational model of slug flow. In: AIChE Annual Spring Meeting, New Orleans.

Clarke, A., Issa, R.I., 1993. A multidimensional computational model of slug flow. Gas–Liquid Flows '93 FED-165, 119–130.

Clift, R, Grace, J.R., Weber, M.E., 1978. Bubbles, Drops and Particles. Academic Press, NY.

Collins, R., de Moraes, F.F., Davidson, J.F., Harrison, D., 1978. The motion of a large gas bubble rising through liquid flowing in a tube. J. Fluid Mech. 89, 497–514.

Davies, R.M., Taylor, G.I., 1950. The mechanics of large bubbles rising through extended liquids and through liquid in tubes. Proc. R. Soc. London A 200, 375–390.

DeJesus, J.D., Ahmad, W., Kawaji, M., 1995. Experimental study of flow structure in vertical slug flow. In: Proc. 2nd Int. Conf. Multiphase Flow, Kyoto, P9-51–P9-55.

Donevski, B., Saga, T., Kobayashi, T., Segawa, S., 1995. An automatic image analysis of two-phase bubbly flow regime. In: Proc. 2nd Int. Conf. Multiphase Flow, Kyoto, P1-21–P1-26.

Dumitresku, D.T., 1943. Strömung an einer Luftblase im senkrechten Rohr. Z. Angew. Math. Mech. 23, 139–149.

Goldsmith, H.L., Mason, S.G., 1962. The movement of single large bubbles in closed vertical tubes. J. Fluid Mech. 14, 52–58.

Grace, J.R., Clift, R., 1979. Dependence of slug rise velocity on tube Reynolds number in vertical gas–liquid flow. Chem. Eng. Sci. 34, 1348–1350.

Griffith, P., Wallis, G.B., 1959. MIT Technical Report No. 15. NONR-1959, 1841.

Griffith, P., Wallis, G.B., 1961. Two-phase slug flow. J. Heat Transfer 83, 307–320.

Kawaji, M., DeJesus, J.M., Tudsoe, G., 1997. Investigation of flow structures in vertical slug flow. Nucl. Eng. Des. 175, 37–48.

Kvernvold, O., Vindoy, V., Sontvedt, T., Saasen, A., Selmen-Olsen, S., 1984. Velocity distribution in horizontal slug flow. Int. J. Multiphase Flow 10, 441–457.

Lunde, K., Perkins, R.J., 1995. A method for the detailed study of bubble motion and deformation. In: Proceedings of the 2nd Internat. Conf. on Multiphase Flow, Kyoto, AV17–AV24.

Mao, Z.S., Dukler, A., 1989. An experimental study of gas–liquid slug flow. Experiments in Fluids 8, 169–182.

Mao, Z.S., Dukler, A., 1990. The motion of Taylor bubbles in vertical tubes: I. A numerical simulation for the shape and rise velocity of Taylor bubbles in stagnant and flowing liquid. J. Comp. Phys. 91, 132–160.

Mao, Z.S., Dukler, A., 1991. The motion of Taylor bubbles in vertical tubes: II. Experimental data and simulations for laminar and turbulent flow. Chem. Eng. Sci. 46 (8), 2055–2064.

Martin, C.S., 1976. Vertically downward two-phase slug flow. J. Fluids Eng., Transactions of the ASME 98, 715–722.

Meisen, R., Boersman, B.J., 1995. Hydrodynamic stability of a sheared liquid film. J. Fluid Mech. 301, 175–202.

Nakoryakov, V.E., Kashinsky, O.N., Kozmenko, B.K., 1986. Experimental study of gas–liquid slug flow in a small-diameter vertical pipe. Int. J. Multiphase Flow 12 (3), 337–355.

Nakoryakov, V.E., Kashinsky, O.N., Petukhov, A.V., Gorelik, R.S., 1989. Study of local hydrodynamic characteristics of upward slug flow. Experiments in Fluids 7, 560–566.

Nicklin, D.J., Wilkes, J.O., Davidson, J.F., 1962. Two-phase flow in vertical tubes. Trans. Inst. Chem. Eng. 40, 61–68.

Polonsky, S., 1998. Ph.D. Thesis, Tel-Aviv University.

Polonsky, S., Barnea, D., Shemer, L., 1999. Averaged and time-dependent characteristics of the motion of an elongated bubble in a vertical pipe. Int. J. Multiphase Flow 25, 795–812.

Singh, G., Griffith, P., 1970. Determination of the pressure drop optimum pipe size for a two-phase slug flow in an inclined pipe. J. Eng. Ind. 92, 717–726.

Shemer, L., Barnea, D., 1987. Visualization of the instantaneous velocity profiles in gas–liquid slug flow. Physicochem. Hydrodyn 8, 243–253.

Tassin, A.L., Nikitopolous, D.E., 1995. Non-intrusive measurements of bubble size and velocity. Experiments in Fluids 19, 121–132.

Tung, K.W., Parlange, J.Y., 1976. Note on the motion of long bubbles in closed tubes — influence of surface tension. Acta Mechanica 24, 313–317.

White, E.T., Beardmore, R.H., 1962. The velocity of rise of single cylindrical air bubbles through liquids contained in vertical tubes. Chem. Eng. Sci. 17, 351–361.